LA-5167-MS

INFORMAL REPORT

Multipass Systems for CO_2 Laser Plasma Heating and Diagnostic Scattering Experiments

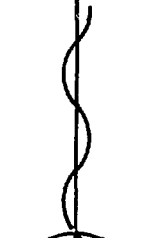

los alamos
scientific laboratory
of the University of California
LOS ALAMOS, NEW MEXICO 87544

UNITED STATES
ATOMIC ENERGY COMMISSION
CONTRACT W-7405-ENG. 36

In the interest of prompt distribution, this LAMS report was not edited by the Technical Information staff.

Printed in the United States of America. Available from
National Technical Information Service
U. S. Department of Commerce
5285 Port Royal Road
Springfield, Virginia 22151
Price: Printed Copy $3.00; Microfiche $0.95

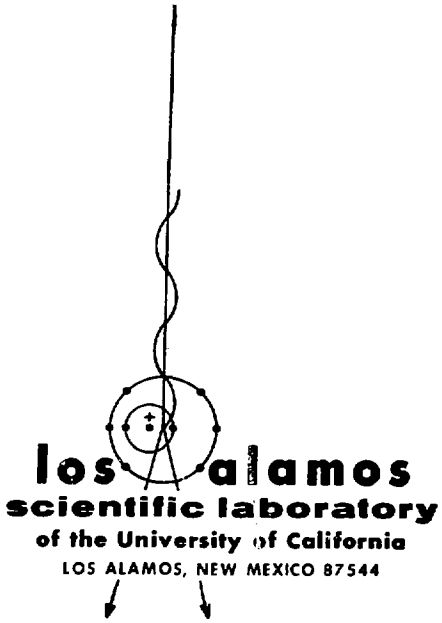

LA-5167-MS
Informal Report
UC-20
ISSUED: February 1973

Multipass Systems for CO_2 Laser Plasma Heating and Diagnostic Scattering Experiments

by

Stanley Humphries, Jr.

MULTIPASS SYSTEMS FOR CO_2 LASER PLASMA HEATING AND DIAGNOSTIC SCATTERING EXPERIMENTS

by

Stanley Humphries, Jr.

ABSTRACT

The interaction between plasmas and the infrared radiation from CO_2 lasers has become of great interest because of possibilities for plasma heating and diagnostic scattering experiments. In this report, calculations are presented on a laser-plasma system in which the plasma is located within a high Q laser cavity, maximizing the useful radiation density. The stability of cavities with the inclusion of a cylindrical pinch plasma is investigated for propagation along and across the column. Conditions are given under which the presence of the plasma is necessary for cavity oscillations, raising the possibility of plasma Q-switching. Calculations are performed on the expected shape of laser modes in the plasma, taking the plasma dynamics into account. It is shown that these modes are unfavorable to heating of the bulk of the plasma, and are unstable against hydro-magnetic kinking. A heating experiment using a small pinch and modest laboratory laser is described that would allow measurement of low density (10^{16}-10^{17} cm^{-3}) laser-plasma interactions and many transport properties of fully ionized plasmas. Feasibility studies are also presented on the use of closed-cavity CO_2 laser scattering to measure the ion temperature in pinches. Experiments demonstrating the behavior of closed cavities in which powers of 200 megawatts were obtained with a 1-joule laser are also described.

I. INTRODUCTION

There has recently been a great deal of interest in the possibility of heating magnetically confined plasmas using pulsed CO_2 lasers.[1] At densities attainable in conceivable pinch devices, the interaction between the plasma and radiation is weak. To alleviate the problem of long absorption lengths, the possibility of allowing the radiation to make many passes through the plasma has been suggested.[1] In this report, a particularly advantageous multiple pass system formed by placing the plasma inside a closed, CO_2 laser cavity will be discussed. Such a system has been described in a previous report and by other authors.[2,3,4] It would lend itself well to a versatile laboratory experiment, but it will be shown that the application of any multiple-pass arrangement to systems in the range of proposed reactors is unlikely.

In a closed laser cavity, all the radiation produced is trapped. Losses are mostly on the mirrors, and can be kept less than 1 per cent for each transit. If a weakly absorbing sample is placed within the cavity, the laser energy would travel through it more than fifty times. This method has been used successfully to enhance second-harmonic generation.[5] A laboratory plasma can be heated uniformly, in this way, by inverse Bremsstrahlung. The application of the closed cavity to another process of small cross section, laser scattering, will also be discussed.

In Section II, the optical characteristics of a laser cavity with an included pinch plasma are investigated. These include the stability of the cavity and the possibility of using an imploding plasma as a laser Q-switch. Modes of propagation of the radiation through the plasma, taking the plasma dynamics into account are derived. It is shown in Section III-A that these modes are generally unfavorable to heating of the bulk of the plasma, and are subject to a hydromagnetic kinking

instability. In Section III-B, a laboratory experiment in which a variety of regimes of laser-plasma heating could be studied is described. Because of the localized heating in such an experiment it would also be possible to study various plasma transport coefficients. Section IV is devoted to a study of a closed cavity laser scattering experiments. It is shown that plasma perturbations of the laser radiation are negligible, and that an enhancement in the available power by about a factor of 30 is possible compared to an open cavity laser. Experimental results are presented demonstrating the behavior of a closed cavity in which an intracavity power of about 200 megawatts was achieved.

II. INTERACTIONS OF A CLOSED CAVITY LASER WITH A CYLINDRICAL PLASMA COLUMN

In this section, a closed cavity laser system enclosing a cylindrically symmetric plasma column will be given a general treatment. Studies include the stability of the laser cavity, the possible use of an imploding plasma to Q-switch the laser, and the expected shape of the laser modes within the plasma. In Section III the results obtained will be applied to the heating of plasmas to reactor parameters and a proposed laboratory scale plasma heating experiment.

A. Stability of a laser cavity containing a short, cylindrically symmetric plasma column.

The simplest intra-cavity plasma heating configuration is shown in Fig. 1. To maximize the interaction , the radiation propagates longitudinally

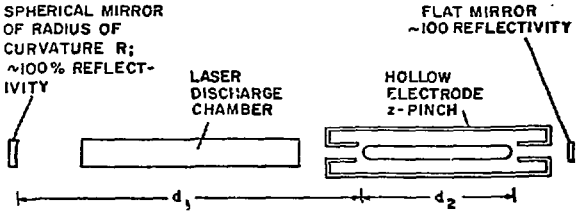

Fig. 1. Simple multiple-pass system.

along the column. A hemispherical cavity is chosen to maximize the volume of the mode within the lasing medium. Additional optics could be introduced to optimize the size of the laser mode at the expense of higher losses. By assuming a short cavity, diffraction can be neglected and a ray optics model will be used. It should be remembered that because of their high gain CO_2 lasers can operate even with an unstable cavity. Sufficient conditions for the inhibition of lasing will be derived in Section II-B.

Figure 2 shows an infinitely repetitive optical cavity equivalent to that of Fig. 1 with appropriate ray transfer matrices[6] entered under the various elements. The plasma is assumed to have a

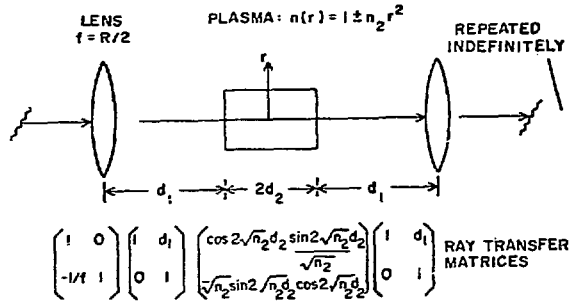

Fig. 2. Optical equivalent of Fig. 1.

length d_2 with sharp axial boundaries. When $\omega_p^2 \ll \omega^2$, the average index of refraction closely equals 1, and reflection at the boundaries is small. Over the cross-sectional area occupied by the laser mode, the radial electron density is approximated by the parabolic dependence

$$n_e(r) = n_{eo}\,(1 \pm \delta r^2)\ . \qquad (1)$$

For $\omega_p^2 \ll \omega^2$, the index of refraction varies radially as

$$n(r) \cong 1 \pm n_2 r^2 \text{ where } n_2 = \delta \left(\frac{\omega_p}{\omega}\right)^2. \qquad (2)$$

For a hollow density distribution (corresponding to a minus sign in Eq. 2) the ray transfer matrix is that given in Fig. 2. For a density distribution decreasing away from the axis (a plus sign) the trigonometric functions are replaced by hyperbolic functions. The total ray transfer matrix for the system is computed by matrix multiplication of the individual elements. The system is stable if the magnitude of the trace of the total matrix is less than two.[6] This implies that

$$\left| \left(1 - \frac{2d_1}{R}\right) \cos 2\sqrt{n_2}d_2 - \left(\frac{1}{R\sqrt{n_2}} + \sqrt{n_2}d_1\left(1 - \frac{d_1}{R}\right)\right) \sin 2\sqrt{n_2}d_2 \right| < 1 \qquad (3)$$

for the hollow density distribution. Here, R is the radius of curvature of the spherical mirror and d_1 is the distance from this mirror to the plasma boundary.

When the product $\sqrt{n_2}\ (2d_2)$ is of the order of unity or larger, refraction effects are significant. For almost all practical cases, density distributions decreasing from the center are unstable. Thus, only hollow distributions, which can usually be obtained during the initial implosion of a pinch, will be of use. For hollow profiles, two special cases of Eq. 3 will be considered. When $\sqrt{n_2}\ (2d_2) = \pi, 2\pi, \ldots$, the condition for stability becomes

$$-1 < (1 - 2d_1/R) < +1 \quad , \qquad (4)$$

equivalent to the result obtained for a normal laser if the length occupied by the plasma is neglected. This occurs because the plasma ray transfer matrix becomes unity, and rays leave the plasma with the same displacement and angle with which they entered. When $\sqrt{n_2}\ (2d_2) = \pi/2, 3\pi/2, \ldots$, the stability condition becomes

$$\left| \frac{1}{R\sqrt{n_2}} + d_1\sqrt{n_2} \left(1 - \frac{d_1}{R}\right) \right| < 1 \ . \qquad (5)$$

When the cavity (excluding the plasma is concentric ($R = d_1$), the system will be stable if $d_1 > 1/\sqrt{n_2}$. For the confocal cavity ($R = 2d_1$), the stability condition is

$$\left| \frac{1}{2\sqrt{n_2}d_1} + \frac{d_1\sqrt{n_2}}{2} \right| < 1 \ .$$

Stability will be achieved only for the singular case of $d_1 = 1/\sqrt{n_2}$.

B. Use of an Imploding Plasma to Q-Switch a Laser Cavity.

The analysis of Section II-A indicates that, if n_2 can be estimated, the optics of the laser cavity can be chosen to allow one of three possibilities: 1) the laser cavity is always stable, 2) the laser cavity is stable only with plasma present, and 3) it is stable when $\sqrt{n_2}\ (2d_2) = \pi, 2\pi, \ldots$ but unstable when $\sqrt{n_2}\ (2d_2) = \pi/2, 3\pi/2, \ldots$. This raises the possibility of Q-switching the laser with the imploding plasma if losses can be made high enough in the unstable limits. During the implosion stage, the quantity $\sqrt{n_2}\ (2d_2)$ increases and could bring the ray transfer matrix through one or more cycles. Under condition 2 (represented by the concentric cavity) the laser could not fire until plasma refractive effects became high enough. This would guarantee that radiation built up in the cavity only when it could be contained in the plasma. Under condition 3 (represented by the confocal cavity) it may be possible to double-pulse the laser, making more efficient use of the available population inversion.

CO_2 lasers typically have high gains ($\gtrsim$ 50 per cent per pass), and it must be shown that losses can be made large in the unstable cases. An analysis has been carried out by Seigman[7] to find self-consistent modes and losses in unstable cavities consisting of two spherical mirrors. This analysis will be generalized here to the case of a repetitive system of arbitrary optical configuration. Seigman finds modes in the geometric optics approximation consisting of spherical wavefronts. Then, based on numerical results of Fox and Li,[8] he assumes that the mode of the unstable cavity is approximately radially uniform. By calculating the extreme rays of the system, one can use a simple gemetric construction to estimate the losses in one pass.

Figure 3a shows one pass of a general laser cavity which can be represented by a ray transfer matrix, $\begin{vmatrix} A & B \\ C & D \end{vmatrix}$, between the entrance plane and the exit plane (the entrance plane for the next pass). The change in displacement of a ray in one pass is calculated with respect to this plane, so it is chosen as the location at which the greatest losses are expected. As in Section II-A, the system is unstable if $(A + D)/2 > 1$. To clarify sign conventions, mirrors are replaced by equivalent lenses so that all rays move from left to right. Referring to Fig. 3b, in the paraxial approximation spherical waves are represented by the ray vector (y, y/r) for diverging waves and (y, -y/r) for converging waves, where r is the radius of curvature.

After one pass through the system, the ray vector is transformed to

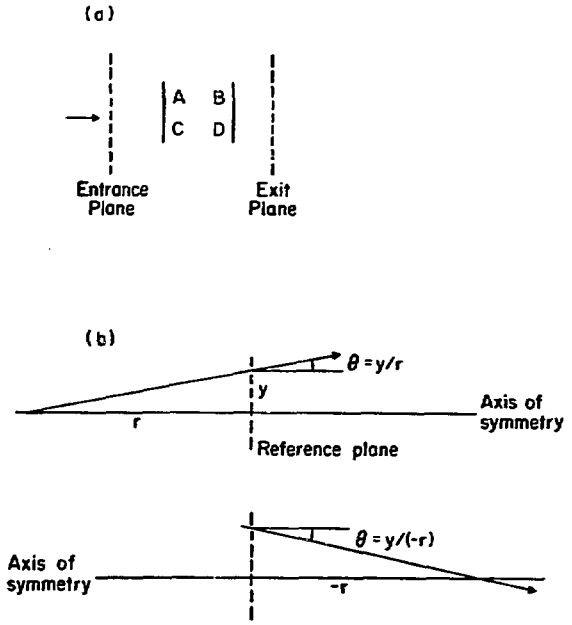

Fig. 3. Conventions for the calculation of modes in an unstable resonator.

$$\begin{bmatrix} y' \\ y'/r' \end{bmatrix} = \begin{bmatrix} Ay + By/r \\ Cy + Dy/r \end{bmatrix} . \qquad (6)$$

For a self-consistent solution, it is required that $r = r'$. This constrains r such that

$$r = \frac{(A-D) \pm \sqrt{(A-D)^2 + 4BC}}{2C} . \qquad (7)$$

The choice of sign gives a solution which either converges towards the axis or diverges. These solutions are identical except for a reversal in the direction of the rays. Only diverging solutions will be considered physically meaningful. Since the determinant of the ray transfer matrix equals one[6], real solutions to Eq. 7 exist only for unstable cavities. Knowledge of r allows calculation of y' in terms of y

$$y' = Ay + By/r . \qquad (8)$$

If y is assumed to be an extreme dimension (i.e., the radius of a mirror), then rays having a displacement greater than y after one pass are lost. The fraction lost per pass is given by

$$t \cong \frac{y'^2 - y^2}{y'^2} . \qquad (9)$$

As an example, the concentric cavity ($R = d_1$) with no plasma present will be considered. We let $d_1 = d_2$ and choose the plane of reference as the spherical mirror. Two passes through this system are shown in Fig. 4a. $y' = 5.9y$, implying almost 100 per cent loss. Note that by reversing the direction of the rays, the diverging solution becomes a converging one. As a second example, we consider the confocal cavity ($R = 2d_1$) with the entrance of the plasma chosen as the plane of reference. The following are assumed: $\sqrt{n_2}\,(2d_2) = \pi/2$, $d_1 = R/2$, and $d_1 = d_2$, so that $\sqrt{n_2}\,2d_1 = \pi/2$. Two passes of the system are shown in Fig. 4b. $y' = (\pi/2)y$, implying about 60 per cent loss per pass. It thus appears that the Q of the laser cavity can be significantly affected by the plasma.

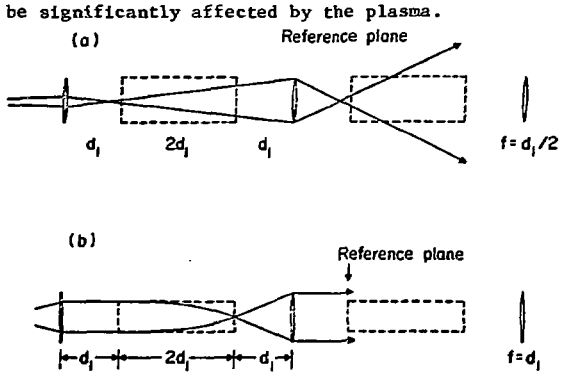

Fig. 4. Examples of modes in an unstable resonator.

C. Self-Consistent Modes of Propagation in a Long Plasma Column.

In long plasmas (such as those contemplated for laser heated reactors[1]) geometric optics calculations will not hold because diffraction becomes important. Even in short plasmas, it is possible to match modes at the plasma boundary to obtain a TEM, z-independent laser mode. In this section, we will calculate the radial dependence of radiation intensity in shock heated and quasi-steady-state regimes for laser modes which have very small change in z over distances comparable to the mode radius, w. Plasma transport coefficients are taken from Reference 9.

The first case to be studied holds either for weak laser pulses (which cause a negligible perturbation in the plasma, $\Delta T_e/T_e \ll 1$) or a shock heating regime where the laser pulse length, t_ℓ, is short compared to the time it takes the plasma to reach a pressure equilibrium. In this case, the shape of the laser mode is determined by the electron density distribution at the time of the laser pulse. This is in turn determined by the external agency responsible for the production of the initial plasma.

If we assume a hollow, parabolic density profile (as in Eq. 1), and that $E_z = 0$, the equation for the laser field becomes

$$\frac{1}{r}\frac{d}{dr}\, r \frac{dE_x}{dr} + k_o^2 \left[\left(1 - \left(\frac{k_z}{k_o}\right)^2 - n_2 r^2\right] E_x = 0, \quad (10)$$

where z-dependent terms have been neglected. This equation is identical to that of the quantum mechanical harmonic oscillator (in a cylindrically symmetric well) and, for modes with no azimuthal variation, has the solution[10]

$$E(r) = E_o\, L_m^o \left(\frac{2r}{w^2}\right) \exp\left(-\frac{r^2}{w^2}\right), \quad (11)$$

where L^o_m is a Laguerre polynomial. Solutions for the first three modes are shown in Fig. 5. In particular, the fundamental mode has a 1/e radius of

$$w = \left(\frac{\lambda}{\pi}\right)^{\frac{1}{2}} \left(\frac{n_o}{n_2}\right)^{\frac{1}{4}} \quad (12)$$

These modes can propagate indefinitely along the plasma without a change in parameters. They can be considered dielectric waveguide modes, with the plasma acting as the waveguide. The neglect of absorption is a good assumption since, in the closed cavity system, only a small portion of the energy need be absorbed per pass. The assumption that the plasma has no motion should be satisfied if the laser pulse, t_ℓ, is short compared to the time it takes the plasma to reach a pressure equilibrium, t_{eq}. This should be of the order of the time it takes for a magnetoacoustic wave to propagate across the dimensions of the laser mode. It is assumed that this time is short compared to other characteristic times such as the electron-ion

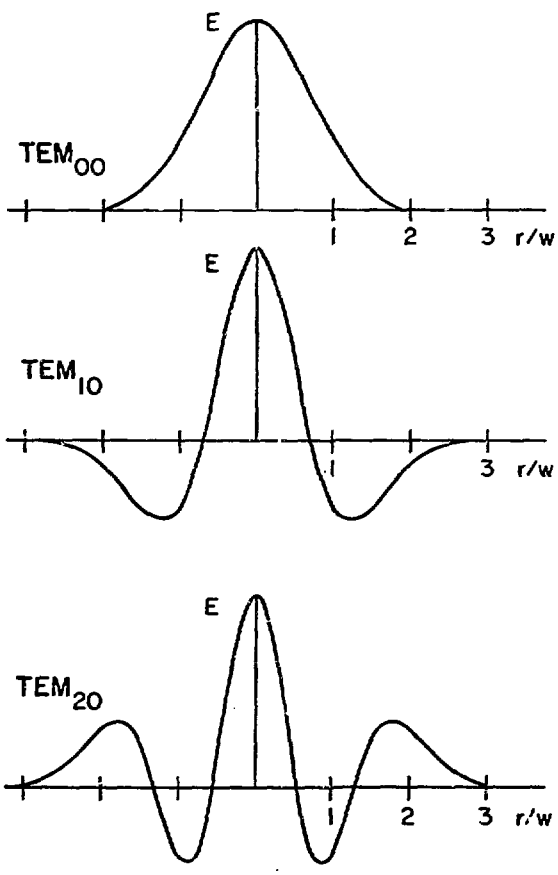

Fig. 5. Laser modes in a parabolic density profile. $w = \left(\frac{\lambda}{\pi}\right)^{\frac{1}{2}} \left(\frac{1}{n_2}\right)^{\frac{1}{4}}$.

equipartition time, t_{ei}, the longitudinal thermal conduction time, t_{thz}, the radial thermal conduction time, t_{thr}, and the plasma confinement time, t_c. Conditions of applicability will be discussed in Section III.

Another interesting case is that in which the laser heating time, t_H, is longer than t_{eq}. In this case, the plasma can be considered in a radial pressure equilibrium, but not necessarily in thermal equilibrium. Here, the radiation maintains a hollow in the electron density distribution by heating and, in essence, determines its own spatial distribution. For the model to hold, we require that $t_{thr} \ll t_{thz}$ and that $t_{thr} \ll t_c$, which are obviously necessary for the practical heating of any equilibrium plasma. A two fluid

model will be used, so that the relative magnitude of t_{ei} is arbitrary. The model will describe a quasi-steady-state situation. Outside the area occupied by the laser radiation, the electron and ion temperatures will approach a constant value, T_{io}. This temperature will raise with time. A steady-state calculation will be approximately valid if $T_{io}/(dT_{io}/dt) \gg t_{thr}$. T_{io} can be estimated from the derived solutions by a calculation of the rate of heat deposition and a knowledge of the size of the surrounding plasma. A non-dimensionalization scheme will be used to facilitate these calculations.

Low or medium β hydrogenic plasmas will be considered in which B^2 does not change greatly over the radial extent of the laser mode, w. Neglecting particle diffusion, the following equations must be satisfied for pressure equilibrium.

$$\frac{d}{dr}(n_e kT_e) = -en_e E_p \,. \tag{13}$$

$$\frac{d}{dr}(n_i kT_i) = en_i E_p \,. \tag{14}$$

$$\frac{1}{r}\frac{d}{dr} r E_p = 4\pi e (n_i - n_e) \tag{15}$$

Here, "i" and "e" refer to ions and electrons and E_p is a DC, thermally supported electric field. An inspection of the above equations shows that

$$\frac{n_e - n_i}{n_i} \sim \left(\frac{\lambda_D}{w}\right)^2 ,$$

which is small for all plasmas and dimensions of interest, so that $n_i \simeq n_e = n$. Adding equations shows that $dp/dr = p/w\,(\Delta n/n)$, where $p = n_e kT_e + n_i kT_i$. Thus the pressure is constant and we can write

$$n(T_e + T_i) = n_o(T_{eo} + T_{io}) \,. \tag{16}$$

With the assumption of approximate neutrality, Eqs. 13, 14 and 15 will be satisfied if E_p is taken as

$$E_p = \frac{k}{e}\left(T_e \frac{dT_i}{dr} + T_i \frac{dT_e}{dr}\right) / (T_e + T_i) \,. \tag{17}$$

The thermally supported voltage will be of the order of kT_e. The thermal equations can be solved with the assumption that the pressure is a constant and that $n_e = n_i$. The radially dependent temperatures can then be used to find the electric field, E_p, that will guarantee equilibrium.

The thermal equations for ions and electrons are

$$\frac{1}{r}\frac{d}{dr} r K_{\perp i}\frac{dT_i}{dr} - \frac{nk(T_e - T_i)}{t_{ei}} = 0 \tag{18}$$

and

$$\frac{1}{r}\frac{d}{dr} r K_{\perp e}\frac{dT_e}{dr} - \frac{nk(T_e - T_i)}{t_{ei}} + S = 0 \tag{19}$$

where z dependences have been neglected. The classical transport coefficients are

$$K_{\perp i} = \frac{(1.2 \times 10^{-14})\, n^2}{T_i^{\frac{1}{2}} B^2} \quad \frac{ergs}{cm^2\ sec} \cdot \frac{cm}{eV} \,,$$

$$K_{\perp e} = \frac{(6.5 \times 10^{-16})\, n^2}{T_e^{\frac{1}{2}} B^2} \quad \frac{ergs}{cm^2\ sec} \cdot \frac{cm}{eV} \,,$$

and

$$t_{ei} = \frac{(1.5 \times 10^{7})\, T_e^{3/2}}{n} \quad sec \,.$$

In all the practical equations given, T_e and T_i are in electron volts, n is in cm^{-3}, E is in statvolts 1 cm, and B is in gauss. The heating source is assumed to be high frequency ohmic heating (inverse Bremsstrahlung) which directly affects only the electrons, given by

$$S = \frac{(1.5 \times 10^{-25})\, E^2 n^2}{T_e^{3/2}} \quad \frac{ergs}{cm^3\ sec} \,. \tag{20}$$

The laser field is of the form $E(r,z,t) = E(r) \exp(\pm ikz - i\omega t + \varphi)$, where E(r) is determined by

$$\frac{1}{r}\frac{d}{dr} r \frac{dE}{dr} + k_o^2 \left(\mu - \frac{4\pi e^2 n}{m_e \omega^2}\right) E = 0 \,. \tag{21}$$

The solutions of Eqs. 18, 19 and 21 present formidable difficulties. Equation 21 is an eigenvalue equation and Eqs. 18 and 19 must satisfy a mixture of boundary conditions at the origin and at large r, which can only be related by a knowledge of the solution of the non-linear problem. A simplification can be made in the computation of the ion temperature. Recognizing that ion thermal conduction will be rapid compared to the rate of heat transfer from the electrons in all practical cases, the ion temperature can be considered constant over the dimensions of the laser mode. The shape of the mode is thus determined by the electron thermal transport properties. Perpendicular electron thermal conduction is usually negligible (since $K_{\perp e}/K_{\perp i} \sim (m_e/m_i)^{\frac{1}{2}}$), but since the resulting modes are narrow, implying large thermal gradients, and the electron-ion heat transfer rate is slow, this process plays a significant role in determining the shape of the laser mode.

Defining "o" quantities at the origin, the following dimensionless variables will be used

$$\tau_e = T_e/T_{eo},\ \tau_{io} = T_{io}/T_{eo},\ \eta = n/n_o,\ \epsilon = E/E_o$$

Radial dimensions are in centimeters. In terms of these, Eqs. 16, 19 and 21 become

$$\frac{A}{r}\frac{d}{dr}\left[\frac{r\eta^2}{\tau_e^{\frac{1}{2}}}\frac{d\tau_e}{dr}\right] - \frac{B(\tau_e-\tau_{io})\eta^2}{\tau_e^{3/2}} + \frac{\eta^2\epsilon^2}{\tau_e^{3/2}} = 0, \quad (21a)$$

$$\eta = \frac{1+\tau_{io}}{\tau_e+\tau_{io}} ,$$

and

$$\frac{1}{r}\frac{d}{dr}\left[r\frac{d\epsilon}{dr}\right] + \omega^2\left[\mu - \left(\frac{4\pi e^2 n_o}{m_e\omega^2}\right)\eta\right]\epsilon = 0, \quad (22)$$

where

$$A = \frac{(6.7\times 10^8)\ T_{eo}^{\ 2}}{B^2\ E_o^{\ 2}} ,\quad B = \frac{(6.7\times 10^5)\ T_{eo}}{E_o^{\ 2}} .$$

In a typical z-pinch plasma, B_θ goes to zero at the origin, while a bias B_z of magnitude comparable to the maximum B_θ must be applied for stability. It can be assumed that in a z-pinch β_θ approximately equals one. In a theta-pinch plasma, β's on the order of 0.5 are typically obtained. Therefore, in either device B_z is given approximately by $B_z^{\ 2}/8\pi \simeq 2n_o kT_{eo}$. We can also define a parameter to be the ratio between the maximum laser field energy density and the plasma energy density, or $\alpha = (E_o^{\ 2}/8\pi)/2n_o kT_{eo}$. A and B can be rewritten

$$A \simeq \frac{10^{30}}{\alpha n_o^{\ 2}} ,\quad B \cong \frac{8\times 10^{15}}{\alpha n_o} . \quad (23)$$

Equations 21a and 22 are solved by a simultaneous numerical integration out from the origin, with the boundary conditions at r = 0

$$\epsilon = 1 ,\quad \tau_e = 1 ,\quad \eta = 1$$

$$\frac{d\epsilon}{dr} = 0 ,\quad \frac{d\tau_e}{dr} = 0 .$$

Values of μ and τ_{io} are chosen by trial and error until a solution is found in which ϵ approaches zero and τ_e approaches τ_{io} for large r. The calculations were performed on a small computer with a CRT graphical output. Eigenvalue decisions were made by the operator. A variety of fundamental mode solutions for $n_o = 10^{17}$ cm^{-3}, classified according to α, are given in Figs. 6 and 7. Plots of ϵ, τ_e, η and E_p for a typical case are given in Fig. 8. Figure 9 shows the TEM_{10} mode.

The constraint on β mentioned above fixes the ratio of the equipartition rate to the thermal conductivity. Increasing α, and hence increasing the heating rate of the plasma with respect to these transport properties, deepens the density well, resulting in a thinner mode. Increasing the average density increases the refractive effects of the plasma, and again the mode becomes thinner. Solutions were also investigated with the introduction of an arbitrary radial pressure variation, $p(r) = p_o(1 - (r/r_p)^2)$. In this case although there are no solutions that remain bounded as $r \to \infty$, it is possible to find solutions that closely approach zero before diverging. The divergence at large r can be interpreted as diffraction losses.

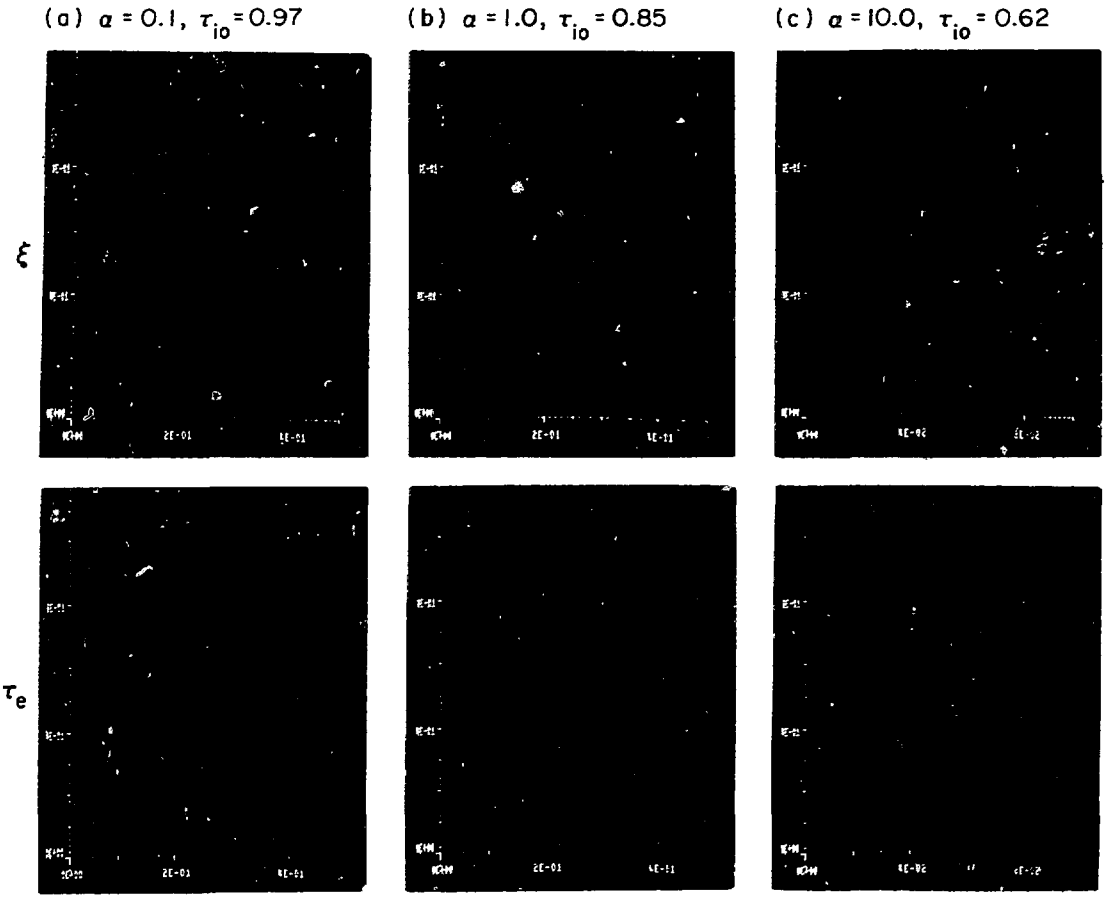

Fig. 6. Steady-state solutions with $n_o = 10^{16}$ cm^{-3}. Abscissa in centimeters.

Approximately bounded solutions can usually be found as long as the fractional decrease of the pressure over the width of the laser mode is small compared to the depth of the electron density well.

III. EXPERIMENTAL APPLICATIONS

A. Closed Cavity Heating of Plasmas to High Temperatures.

There have been proposals to heat pinch plasmas to reactor temperatures using lasers.[1,11] In this section a number of the difficulties involved in this process will be discussed. Some of the problems, such as the small cross-sectional area of laser modes in the plasma and the compressed radiation instability, may also appear in open cavity schemes, raising serious questions about the feasibility of laser heated reactors. Other problems, such as mirror damage and Faraday rotation, will be common to all multiple-pass schemes.

The greatest difficulty in any multiple-pass system is that of mirror damage. The high power levels, while advantageous to the heating process, must somehow be turned back into the plasma. If E_ℓ represents the available laser energy, and L is the length of the entire system, then the maximum power incident on the mirrors is $P_{max} = E_\ell\, c/L$. E_ℓ must be greater than the final plasma energy. For $E_\ell = 10^6$ joules and L = 100 meters, $P_{max} = 3 \times 10^{12}$ watts. Mirrors are currently available that will withstand power levels of 5×10^9 watts for a 200 nonosecond pulse. A mirror with an area of 6000 cm^2 would be needed. The problem remains of how to couple a laser mode of less than 1 cm^2, determined by a rapidly changing plasma, with a mirror of such large area. Solid mirrors will

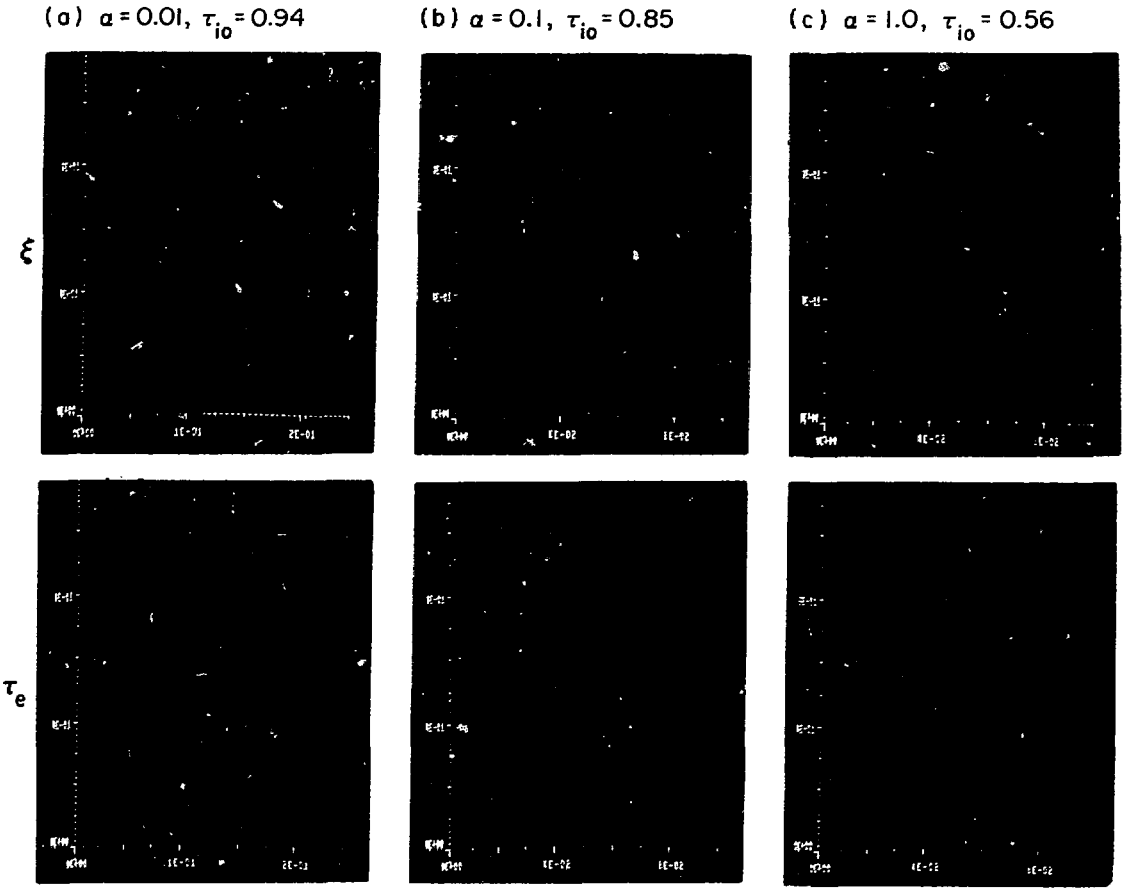

Fig. 7. Steady-state solutions with $n_o = 10^{17}\,cm^{-3}$. Abscissa in centimeters.

probably be necessary because of the large radiation pressures. The force on the end mirrors is given approximately by force (in kilograms) = $E_\ell/10L$. For the parameters given above, the force will be about 1000 kg. The mirrors will probably have to be located within the vacuum chamber, since it would be unlikely that dielectric coated transmitting windows could withstand the expected power levels. Brewster windows could not be used because of the large Faraday rotation expected on each pass.

Multiple-pass systems have some decided advantages over single-pass systems if the above problems could be solved. For efficiency, a single-pass reactor must be made at least two absorption lengths long, assuming that there are lasers at each end. A multiple-pass system could be made a fraction of an absorption length long and still absorb the greater part of the available radiation. An added advantage, besides a decrease in length, is that heating will be longitudinally uniform. In single-pass systems, on the other hand, heating will be peaked at the ends of the plasma. Since this represents a larger proportion of high order thermal diffusion modes, longitudinal thermal conduction is greatly increased. This thermal distribution also increases particle end losses. Another advantage of the multiple-pass system is that, for the same available energy, higher radiation densities can usually be obtained. This will be useful in attempts to shock heat a plasma, as discussed below.

The closed-cavity system is optimal in many respects for laser-plasma heating. On the other

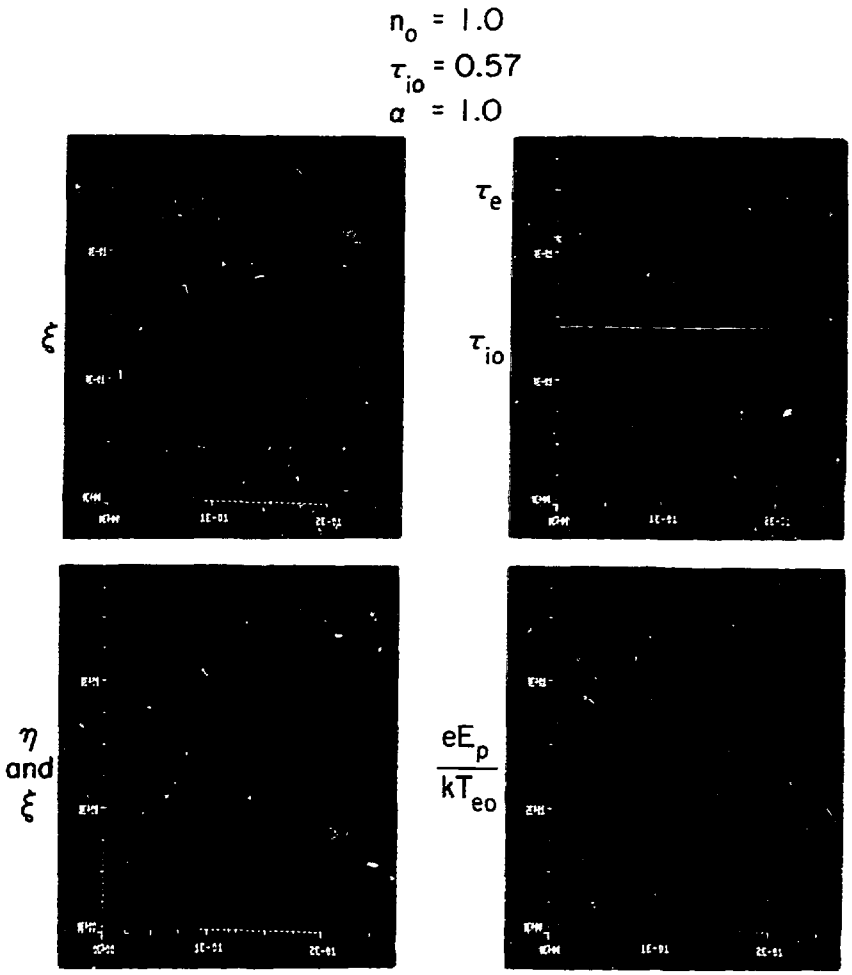

Fig. 8. Steady-state solution showing ξ, τ_e, η and E_p. Abscissa in centimeters.

hand, it will be shown below that even for this system, a number of problems arise which make the prospects of obtaining a high temperature, magnetically confined plasma by laser heating quite remote.

1. The Shock Heating Regime. A regime of shock heating is expected when laser heating causes the plasma pressure to rise faster than the plasma can reach pressure equilibrium, or $t_H < t_{eq}$. This is probably the most advantageous way to heat the plasma. Collective effects can contribute to ion heating at faster rates than the relatively slow collisional equipartition. As shown in Section II-C, if $t_\ell < t_{eq}$, the shape of the laser mode is determined by the initial electron distribution, which can be controlled externally. As t_ℓ becomes longer, the mode will become radially thinner as the radiation begins to form a well in the density. The limit of this process is given by the steady-state calculations of Section II-C.

The equilibrium time is approximately the time necessary for a magnetoacoustic wave to propagate across the dimension of interest, or $t_{eq} \sim w/V_A$. A plot of t_{eq}/w is given in Fig. 10a. The heating time scale is given approximately by $t_H = T_e/(dT_e/dt)$. The time derivative of T_e is calculated by assuming inverse Bremsstrahlung heating and neglecting losses, so that $(dT_e/dt) \simeq S/nk$, where S is given by Eq. 20. The heating

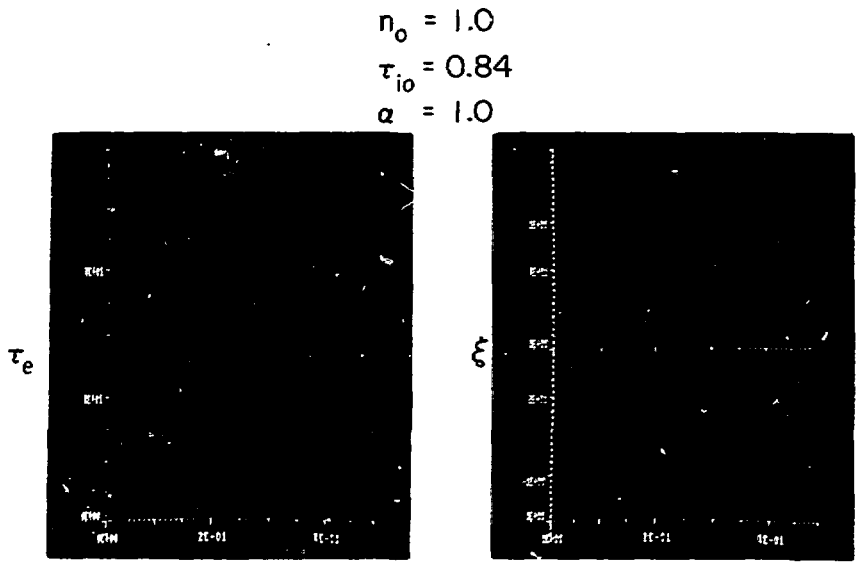

Fig. 9. Steady-state solution. TEM_{10} mode. Abscissa in centimeters.

time is found to be

$$t_H \approx \frac{T_e^{3/2}}{E_o^2 n(10^{-15})} \qquad (24)$$

A plot of t_H for various plasma parameters is given in Fig. 10b.

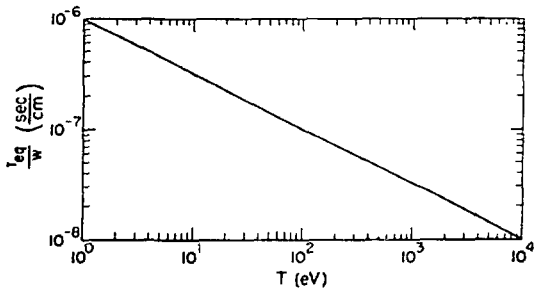

Fig. 10a. Pressure equilibration time, assuming $B \sim \sqrt{8\pi nkT}$.

With low temperature plasmas, it should not be difficult to fulfill conditions for shock heating, but it is doubtful whether this can be done for reactor type plasmas. For example, consider the problem of heating a plasma from 5 keV to 10 keV. The plasma has energy density $\sim 2\, n_o kT_{eo}$ and cross-sectional area A_p. The radiation has an energy density $\sim E_o^2/8\pi$ and area A_ℓ. The total laser energy can not be greater than the final plasma energy, so it is found that $E_o^2 \sim (8\pi)\,(2n_o kT_{eo})A_\ell/A_p$,

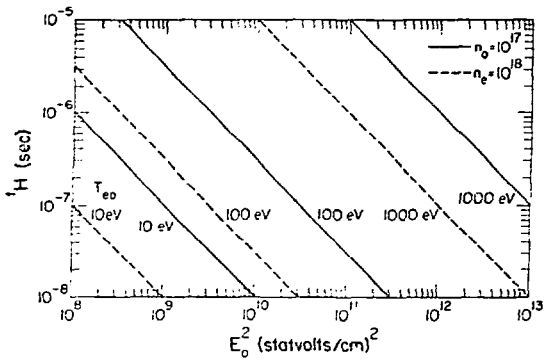

Fig. 10b. Laser heating time, t_H.

where $T_{eo} = 10$ keV. Here the optimal case of a closed cavity, in which all the available energy appears in the plasma at one time, is assumed. Taking $n_o = 5 \times 10^{17}$ as a maximum attainable density and $A_\ell/A_p = 10^{-2}$, we find that $t_H = 10^{-7}$ seconds. If the plasma has a radius of 3 cm, w = .3 cm and $t_{eq} = 3 \times 10^{-8}$ seconds. It is thus probable that the plasma will be in a pressure equilibrium.

2. The Equilibrium Regime. In Section II-C, a fluid model has been used to describe the radial variations of plasma properties for a plasma in pressure equilibrium with quasi-steady-state heating. The fluid model should be valid if the following conditions are satisfied. 1) The electrons and ions have approximately Maxwellian

distributions at their respective temperatures, T_e and T_i. 2) The ion gyroradius must be smaller than dimensions of interest. The first condition will be satisfied because of the relative length of t_{ei} and the steady-state nature of the problem. Taking $B^2 \simeq 8\pi(2nkT)$, the ion gyroradius is given by $r_g \simeq 6/(nr_e)^{\frac{1}{2}}$. At 10^{16} cm^{-3}, r_g = .1 cm, and at 10^{17} cm^{-3}, r_g = .036 cm. r_g will be smaller for $T_i < T_e$. In the range of interest, most of the solutions found will have w smaller than r_g. (See Fig. 11). Thus, r_g plays an important part in determining the width of the laser mode and, as a general rule, self-consistent laser modes will have a width comparable to r_g if there are no anomalous heat transport mechanisms.

The most interesting feature of the solutions of Figs. 6 and 7 is the width of the laser modes. The FWHM is plotted in Fig. 11 as a function of α for $n_o = 10^{16}$ cm^{-3} and 10^{17} cm^{-3}.

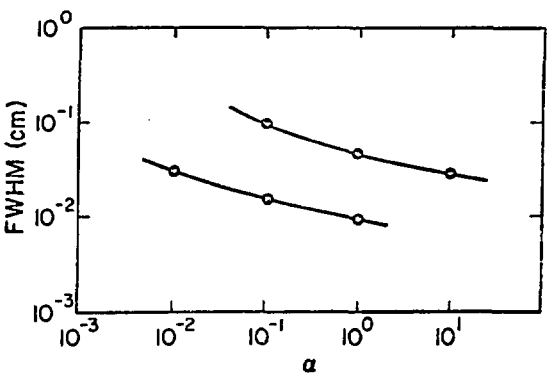

Fig. 11. FWHM of steady-state solutions versus α.

Note that over a wide range of α, the modes have $w < r_g$, and thus the widths will be determined mainly by r_g. The following considerations give an idea of the range of α. At early times in the heating, with a closed cavity, it is probable that the laser energy per unit length is larger than the plasma energy per unit length, since the total radiation energy must be larger than the final plasma energy. This, combined with the fact that the cross-sectional area of the radiation must be smaller than the plasma area, indicates that α must be large compared to 1. At later times when the radiation has decayed and the plasma energy has presumably risen, α can be comparable to 1.

In one respect, these results are favorable. The laser radiation should easily be able to maintain its own equilibrium density well, and thus be transported through the center of the plasma with small loss. On the other hand, there are decided disadvantages. In most cases, the laser radiation is confined to a small cross-sectional area compared to the plasma. This will cause an elevated electron temperature at the center that inhibits absorption. Depending on the mode width and the size of the plasma, less than 1 per cent of the electrons may be directly heated. This heat can be transferred to the main body of the plasma only by the slow processes of electron-ion collisional transfer followed by ion transverse conduction, or electron transverse conduction. The resulting heating rates will be far slower than those calculated on the basis of spatially homogeneous models. This effect becomes worse as the density increases. Microinstabilities driven by the large thermal gradients would be beneficial since transverse heat conduction would be increased, and the laser modes widened.

On the question of the gross stability characteristics of radiation columns contained within cylindrical plasmas, it will be shown below that the derived solutions are stable against self-focusing, but, on the other hand, it will be shown in Section III-3 that such configurations are inherently unstable to m = 1 hydromagnetic modes. Self-focusing, implies a tendency for the derived equilibria to become spontaneously thinner. Two equilibria having the same plasma characteristics external to the laser mode (designated by "∞") with slightly different α's, α and α', such that $\alpha' > \alpha$, will be compared. The solution with α' will have a higher E_o and be thinner. If this solution has a lower total field energy (caused by a decrease in the area occupied by the laser mode), then in an actual perturbation there would be extra field energy available above that needed to maintain the steady-state, and the compression would continue. In comparing solutions, some care must be taken, since the dimensionless variables are defined at the origin. The solutions should have $n_\infty = n_\infty'$, and $T_{io} = T_{io}'$. This implies the following relationships

$$\frac{n_o'}{n_o} = \frac{(1 + \tau_{io})}{(1 + \tau_{io}')} ,$$

$$\frac{\text{Field energy}'}{\text{Field energy}} = \frac{\alpha' n_o' \tau_{io}}{\alpha n_o \tau_{io}'} \frac{\int \epsilon^2 \, 2\pi r dr}{\int \epsilon^2 \, 2\pi r dr} .$$

Since τ_{io}' is not known before the calculation, n_o' must be found in an iterative fashion. For low α's, τ_{io} always equals approximately 1, so it can be assumed that $n_o' = n_o$. Two cases were studied. 1) $n_o = 1.$, $\alpha = 1.$ and $\alpha' = 1.2$; 2) $n_o = 10.$, $\alpha = 1$, and $\alpha' = 1.2$. In both cases the field energy increased, in number 1 by 12% and in number 2 by 16%. It can safely be concluded that the derived solution will be stable against self-pinching.

3. Radiation Driven Firehose Instability. In this section, inter-active hydromagnetic instabilities between a column of radiation and its containing plasma will be considered. The geometry will be the type expected in the heating of a cylindrical plasma by intense laser radiation, and is shown in Fig. 12a. As mentioned above, during early stages of the heating it is probable that the radiation energy per unit length, $u \cong (E_o^2/8\pi)A_\ell$, will be greater than the plasma energy per unit length, $2nkTA_p$. This case will be treated, and the case where the energies are comparable will be discussed qualitatively.

The closed-cavity situation is the easiest to calculate. The available radiation energy rapidly enters the cavity and then rings out. Considering a length of the radiation column, L, for an adiabatic change in L the energy of the radiation contained in L, E, changes according to

$$\frac{\Delta E}{E} = - \frac{\Delta L}{L} . \qquad (25)$$

If the length of the cavity is changed by moving the end mirrors, the energy goes into work done on the mirrors by the radiation pressure, $\Delta E = P_{rad} \Delta L$.

An m = 1 perturbation is introduced into the plasma as shown in Fig. 12b. Before the perturbation, it is assumed that the laser mode is approximately TEM, which holds when $(\lambda/w)^2 \ll 1$. In this case the radiation exerts negligible transverse force on the plasma since the Poynting vector has a small transverse component. With the introduction of the perturbation, the loss of energy of the radiation couples into increased sideways motion of the plasma, since the radiation can now exert significant transverse force on the plasma. The perturbation is taken to have the form $y(z,t) = \xi(t)\cos kz$, where $\xi k \ll 1$, $k^{-1} \ll L$, and $k^{-1} \gg w$. The last condition guarantees that for small perturbations the radiation column will be approximately the same in cross-section as for the unperturbed case (i.e., z-derivatives are small and can be neglected in the calculation of the transverse mode.) The change in length of the plasma and radiation column is given by $\Delta L/L = \frac{1}{4}(\xi k)^2$, and hence the change in energy is $\Delta E = -\frac{1}{4}(\xi k)^2 uL$. This energy goes into kinetic energy as the plasma undergoes free transverse acceleration. Even if the plasma were stabilized against m = 1 modes before the introduction of the radiation, by the assumption that the radiation energy is much larger than the plasma energy, these restoring forces will be small compared to the destabilizing force of the radiation, and can be neglected in the first approximation. If the plasma has a transverse velocity of $dy/dt = \cos kz \, (d\xi/dt)$ and a mass per unit length of ρ, then the kinetic energy of the plasma is in the length L is

$$\text{K.E.} = \int_o^L \left(\frac{1}{2} \rho \left(\frac{d\xi}{dt} \right)^2 \right) \cos kz dz \simeq \tfrac{1}{4} \rho L \left(\frac{d\xi}{dt} \right)^2$$

Equating the two energies and solving for ξ gives $\xi = \xi_o \exp(\gamma t)$ where $\gamma = k(u/\rho)^{\frac{1}{2}}$. If (Radiation energy)/(Plasma energy) = m, then the growth rate is given by $\gamma = kv_{thi}(m)^{\frac{1}{2}}$, where v_{thi} is the ion thermal velocity. Since k^{-1} must be less than the length of the plasma, the growth time will be short compared to the containment time. As the perturbation grows, the neglect of z-derivatives in the calculation of the transverse laser mode will become a bad approximation, and a point will be reached where the radiation breaks out of the plasma.

A physical picture of the origin of the force can be gained from a simple photon model. In the unperturbed situation, since there is no transverse force, the photons must travel in straight lines along the inside of the plasma. There are $u/h\nu$

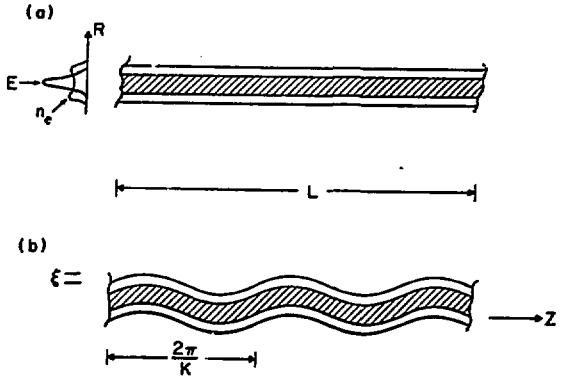

Fig. 12. Geometry for calculation of instability. (a) Radiation column contained by plasma. (b) Introduction of m = 1 perturbation.

photons/length. If a perturbation fulfilling the conditions mentioned above is introduced, the photons still travel in a straight line with respect to the plasma column, but follow a sinusoidal path in space, as shown in Fig. 13a. On each photon there is a centrifugal force directed outwards along the radius of curvature of the path, a, given by $F_a = h\nu/a$. This can be broken up into a longitudinal and transverse component, $F_\ell = F_a \sin\theta$, and $F_t = F_a \cos\theta$, where $\theta \simeq dy/dz$. dy/dz is of the order of ξk, so that F_ℓ can be neglected, and $F_t \simeq F_a$. The radius of curvature is given to first order in ξk by $a \cong (d^2y/dx^2)^{-1}$. Taking all the above into consideration, the force per unit length exerted by the photons divided by the mass per unit length is $F_t/\rho = \xi k^2 h\nu(u/h\nu)\ \cos kz/\rho = k^2 u/\rho$. When equated to the acceleration of the plasma, $d^2\xi/dt^2$, the same growth rate as above is obtained.

Whereas the m = 1 instability tends to lengthen the radiation column, the m = 0 instability would tend to shorten it. Thus the presence of a radiation column will give a plasma additional stability against this mode. The photon interpretation of this phenomenom is shown in Fig. 13b. When the radiation energy is comparable to or less than the plasma energy, the growth rates of the kink instability will be reduced if the plasma is stable without the radiation present.

B. Closed Cavity Heating of Laboratory Plasmas.

Although of doubtful use as a reactor, the closed cavity heating of a laboratory plasma by a CO_2 laser opens many experimental possibilities. In addition to the ability to study high frequency

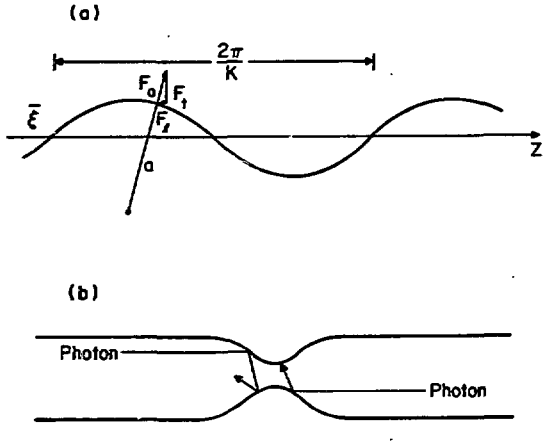

Fig. 13. Photon interpretation of firehose instability. (a) Path of photon through a hollow plasma column with an m = 1 perturbation. $\xi k << 1$. $y = \xi \cos kz$. (b) Hollow plasma containing a radiation column with an m = 0 instability.

heating mechanisms in a controlled manner, it would also be possible to use the spatially localized heating to measure thermal transport coefficients of high β plasmas.

As an example, the heating of a hydrogenic, stabilized z-pinch plasma with $B_z \sim 2n_o kT_{eo}$ will be considered. The plasma has length $d_2 = 60$ cm and cross-sectional area $A_p = 4$ cm^2. The laser has a maximum energy E_ℓ determined by the onset of mirror damage. The cavity length is L = 4 m, and the mirror loss per pass is taken as t = 1%, allowing for one intercavity mirror as well as the end mirrors. If the radiation were spread out over an area A_m on the mirrors, then the maximum power per unit area would be given as $P_{max}/A_m = E_\ell c/A_m L$. For $A = 8$ cm^2 and a maximum permissible power density of 500 megawatts/cm^2, $E_\ell \leq 50$ joules.

The following model gives a rough idea of acceptable plasma parameters. n and T_e are taken to be the plasma density and electron temperature averaged over the heating process and the volume of the plasma, V = 240 cm^2. In order that the plasma heating be significant, it is required that the absorbed laser energy be greater than nkT_eV. The fraction of laser energy lost per pass that goes into heating the plasma is given by

$$f = \frac{(d_2/L_{ab})}{(d_2/L_{ab}) + t} \qquad (26)$$

where L_{ab} is the absorption length for inverse Bremsstrahlung. If L_{ab} is averaged over the absorption process, this represents the fraction of the total laser energy that goes into the plasma. The condition mentioned above becomes $fE_\ell \geq nkT_eV$. Limiting curves of acceptable parameters are plotted in Fig. 14a. Figure 14b gives f for the three curves of Fig. 14a. Easily obtainable densities from 10^{16} to 10^{17} cm^{-3} allow efficient use of the laser energy and investigation of a wide range of temperatures. Since $L_{ab} \sim Z^{-2}$, the results will be even more optimistic for higher Z plasmas. Plasma densities necessary for strong refractive effects, discussed in Section II-A, are in the same range. For instance, with a density hollow of 10% over a 1 cm radius, δ of Eq. 1 equals 0.1 cm^{-2}. For CO_2 radiation and a density of 10^{16} cm^{-3}, $n_2 = 10^{-4}$cm^{-2}, so that $\sqrt{n_2}\,(2d_2) = 1.2$. Refractive effects become stronger at higher densities.

Large radiation densities that will allow shock heating are easily obtainable. For instance, if the laser mode has a cross-sectional area A = 1 cm^2, then E_o^2 (statvolts/cm) = $(6 \times 10^5)\, E_\ell$ (joules). With E_ℓ = 20 joules, $E_o^2 = 1.2 \times 10^7$ statvolts/cm.

The classical time scales of interest for low temperature, hydrogenic pinch plasmas are plotted in Figs. 15a, b, c, d, e, f. These include t_{ei}, t_H, t_{eq}, t_{thr}, t_{thz}, and the confinement time, t_c. The last quantity is given approximately by $t_c = \frac{1}{2}d_2/v_{thi}$. The plasma lifetime will probably be shorter because of instabilities, but t_c gives an idea of the degree on constancy of the plasma over the other times. The time scales obey the following scaling laws:

$$t_{ei} \sim \frac{m_i\, T_e^{3/2}}{n_e\, Z^2} \qquad (27)$$

$$t_H \sim \frac{T_e^{\,6/2}}{E_o^{\,2}\, n_e\, Z^2}$$

$$t_{eq} \sim \frac{w\sqrt{m_i n_i}}{B}$$

$$t_{thr} \sim \frac{T_i^{\frac{1}{2}}\, w^2\, B^2}{A_i^{\frac{1}{2}}\, Z^2\, n_i^{\,2}}$$

$$t_{thz} \sim d_z^{\,2}\, n_e Z/T_e^{\,s/2}$$

$$t_c \sim d_2/\sqrt{T_i/A_i}$$

A wide latitude of experiments is possible. Assuming that densities between 10^{16} and 10^{17} cm^{-3} and temperatures between 5 and 30 eV are accessible, it would be possible to study heating in both the shock and steady-state regimes. For example, at T_e = 10 eV, n = 10^{17} cm^{-3} and $E_o^2 = 10^7$ statvolts/cm, $t_{eq} = 1.5 \times 10^{-7}$ sec for w = .5 cm while $t_H = 3 \times 10^{-8}$ sec. For the steady state regime, at T_e = 30 eV, $n_e = 10^{16}$, and $E_o^2 = 5 \times 10^{18}$ statvolts/cm, $t_{eq} = 10^{-8}$ for w = .5 cm and $t_H = 10^{-6}$ sec. At the same time $t_c = 5.5 \times 10^{-6}$ sec and, since f is small, the e-folding time of the laser pulse, t_ℓ, is a maximum of 1.2×10^{-6} sec. Throughout the entire

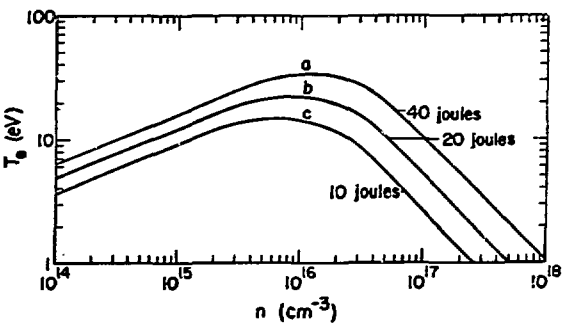

Fig. 14a. Limiting curves of maximum T_e for $E_\ell = E_o$. Plasma length: 60 cm, Plasma area: 4^{P}cm^2, Mirror losses: .01.

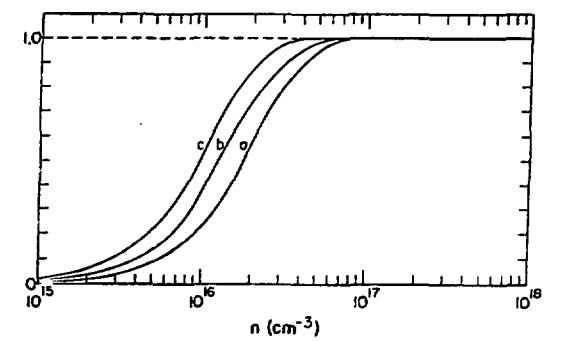

Fig. 14b. Fraction of available energy absorbed in plasma for the curves of 14(a).

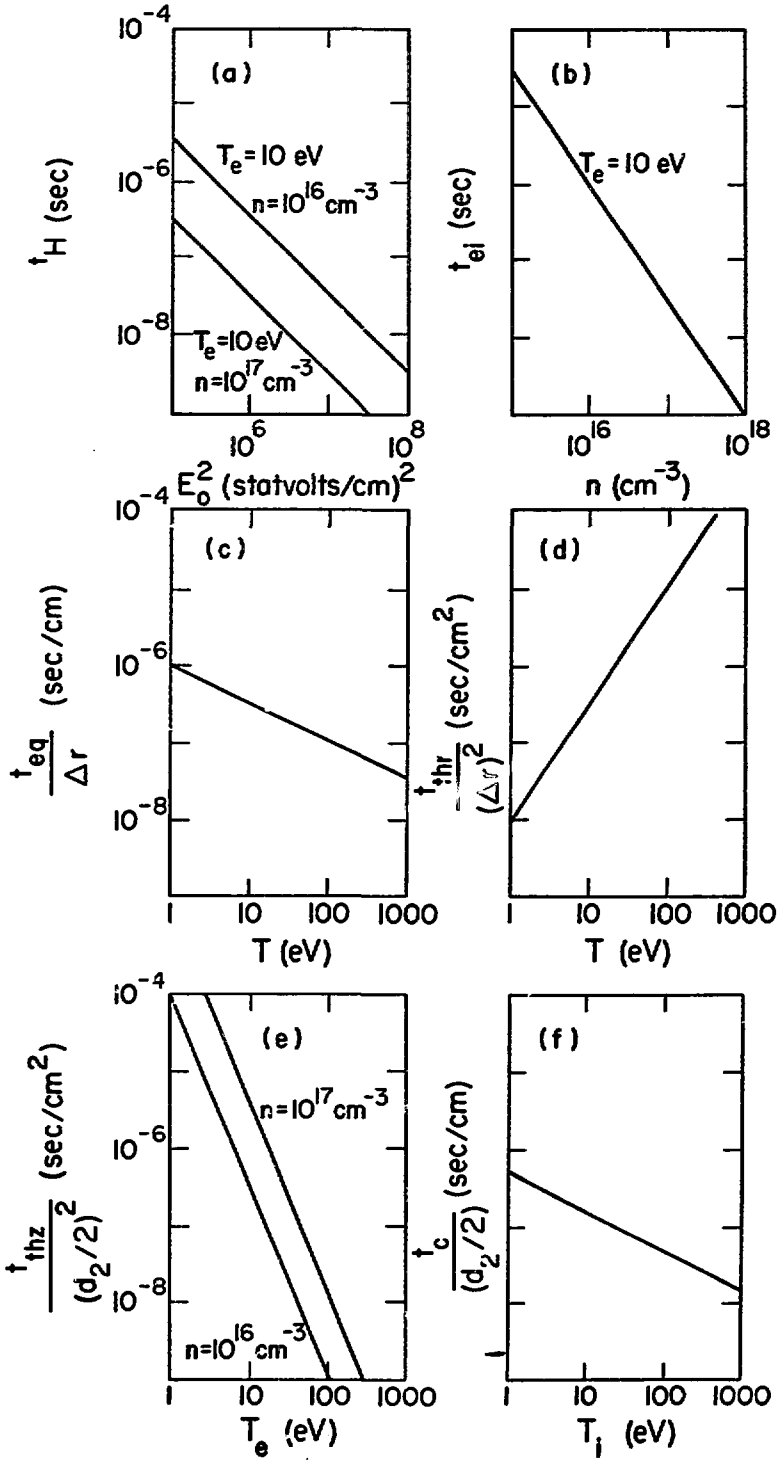

Fig. 15. Characteristic time scales for low temperature plasmas.

range of parameters, $t_{thz} \gg t_{thr}$. In the steady-state regime it is possible to lower E_o^2 to keep the thermal perturbation small and hopefully observe classical transverse heat conduction, or use a larger E_o^2 to search for anomalous effects. At low temperatures it is possible to achieve extreme shock heating where $t_\ell < t_{eq}$. $t_{eq} \sim T^{-\frac{1}{2}}$, while decreasing T can bring f close to 1, so that the radiation decays in a small number of transits ($L/c = 1.3 \times 10^{-8}$ sec). In all of these, the use of higher Z plasmas will increase the resistivity. In particular, since t_H has a Z^{-2} dependence, it should be easier to obtain shock heating. At lower values of E_o^2, the steady-state model will hold quite well since t_H, t_{thr}, and t_{ei} all scale as approximately Z^2, and are thus much shorter than t_{thz} and t_c.

Finally, experiments on stability could be performed. In a z-pinch without a longitudinal field, the m = 0 mode has a faster growth rate than the m = 1 mode and usually destroys the column. According to Section III-A-3, the addition of a trapped radiation column should reverse this behavior. This would provide a good demonstration of the stability effects of trapped radiation.

Figure 16 shows two ways in which a closed-cavity experiment could be carried out. The first is a true closed cavity with the lasing medium included. The results of Section II-A can be applied. With each pass through the plasma, the polarization of the radiation is rotated an angle

$$\theta = \frac{L}{2c}\left(\frac{eB_z}{m_e c}\right)\left(\frac{\omega_p}{\omega}\right) \qquad (28)$$

For example, at $n = 5 \times 10^{16}$ cm^{-3}, L = 60 cm, and B_z = 4500 gauss, $\theta = 23^\circ$. This rules out the use of Brewster windows to separate the lasing medium from the plasma vacuum chamber, since the radiation is expected to make many passes through the plasma and large deviations from the favored polarization can result. A possible substitution is a dielectric coated transmission window, although losses will be increased and care must be taken against radiation damage. A second possible configuration (Fig. 16b) is a partially open cavity with a small filling hole. There would be little feedback from the plasma to the laser, and the mirrors could be located within the vacuum chamber.

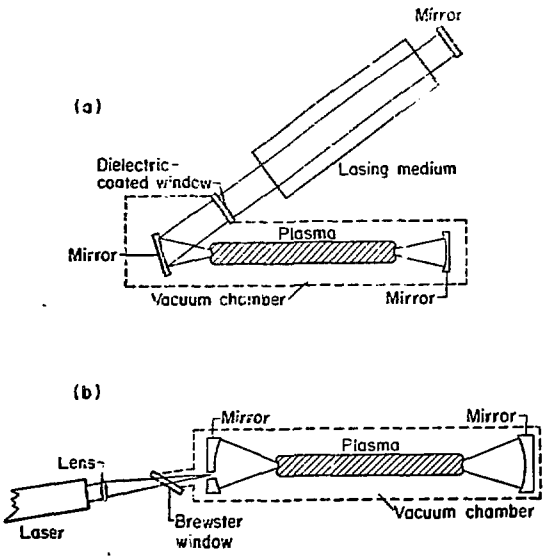

Fig. 16. Closed cavity heating configurations. (a) Interactive closed cavity. (b) Non-interactive closed cavity.

IV. CLOSED-CAVITY CONFIGURATIONS FOR CO_2 LASER SCATTERING EXPERIMENTS

A. Characteristics of a Closed-Cavity CO_2 Laser Scattering Experiment.

The scattering of laser light has become a familiar means to measure plasma distribution functions. In this section the potential use of CO_2 lasers in a closed cavity configuration will be discussed. The CO_2 laser has a number of advantages over the conventionally used ruby laser. 1) The longer wavelength of the CO_2 laser makes it possible to measure features of the ion distribution function without the use of excessively small scattering angles. When the quantity $k_o \lambda_D \sin(\theta/2) > 1$, the frequency spread of the scattered radiation is caused by the Doppler shift induced by ion motion.[12] Here, θ is the scattering angle, λ_D is the Debye length of the plasma, and k_o is the incident wavenumber, fifteen times larger than that of the ruby laser. A plot of $k_o \lambda_D \sin(\theta/2) = 1$ is given in Fig. 17. 2) When used in a closed cavity configuration, CO_2 lasers can produce a useful power equal to that of ruby lasers costing 10 to 20 times as much. 3) Photoconductive detectors for $\lambda = 10.6$ microns are comparable in cost and have higher theoretical efficiencies that red-

sensitive photomultipliers. 4) CO_2 lasers lend themselves well to closed-cavity oscillation in a low order mode because a) the area of a laser mode is proportional to the wavelength, b) the lasing medium, being gaseous, is not susceptible to radiation damage, and c) they have very high gain.

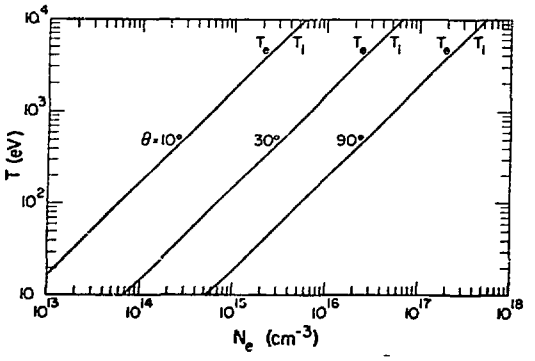

Fig. 17. Scattering regimes for 10.6 micron radiation. $k\lambda_D = 1$

Figure 18 shows the type of set-up that will be considered. The closed-cavity is divided into two parts, one containing the lasing medium and the other containing the plasma, illuminated transversely to minimize perturbations of the radiation. The plasma section of the cavity is chosen to be concentric to focus the radiation to a small spot. For single mode operation, the requirements for long mirror life limit the circulating power to about 250 megawatts. This can easily be obtained with about 1-2 joules of available laser energy, as will be shown in Section IV-C. Losses are mainly due to absorption on the mirrors. Transverse diffraction losses are controlled by a limiting aperture in the lasing section of the cavity, far from the scattering volume. There will be scattering from the mirror surfaces, but this is small for a good mirror and can be absorbed by proper placement of the mirrors. Stray radiation producing a spurious centerline signal may be comparable or smaller than that resulting from a conventional beam dump.

B. Plasma Perturbations

There are two ways in which the plasma could perturb the laser radiation to interfere with the experiment. 1) Changes in the plasma density could

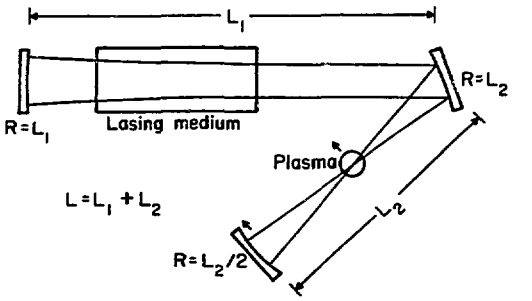

Fig. 18. Closed cavity scattering experiment.

de-tune the frequency of the radiation in the passive cavity. 2) Refractive effects could change the optics of the cavity. It will be shown that both of these are negligible.

Because of rapid collisional transfer of rotational energy, high pressure CO_2 lasers emit in a single transition. Thus, a high gain cavity can rapidly be filled with radiation of a single frequency. During the slower passive decay of the cavity, changes in the density of the plasma can change the frequency of the radiation according to

$$\frac{\Delta\omega}{\omega} = \frac{\Delta L}{L} = \frac{\Delta \int ndz}{\int ndz} \quad , \tag{29}$$

where L is the optical length of the cavity. For example, in a 2 m cavity the decay of a 10^{16} cm^{-3} plasma of dimension 2 centimeters will cause $\Delta\omega/\omega = 10^{-6}$. On the other hand, the ion Doppler induced frequency spread from a 10 eV plasma gives $\Delta\omega_{\frac{1}{2}}/\omega \simeq 1.7 \times 10^{-4}$. Therefore, cavity de-tuning should be a negligible effect.

Refractive effects from the plasma can interfere with the optics of the laser cavity. On the other hand, since the plasma is located at a focus of the radiation, it would be expected that the effects are small. Consider a plasma with a sharp boundary at r_p. It can be shown that for paraxial rays, the plasma acts as a negative cylindrical lens of focus length $f = -r_p \omega^2/\omega_p^2$. For a plasma with $n = 10^{16}$ cm^{-3} and $r_p = 1$ cm, $f = -10$ meters for CO_2 radiation. This is long compared to other focal lengths expected in the system. For example, consider the concentric part of the cavity to have

L = 50 cm, and the plasma to be displaced transversely a distance 0.5 cm as shown in Fig. 18. Then, the radiation falling on mirror 3 should be displaced a distance of about .1 mm, which should have a negligible effect on laser operation.

C. Preliminary Experimental Results

The expected behavior of a high-Q laser cavity is shown in Fig. 19. After the gain switching time, there is a rapid increase in radiation to a maximum power level of $P_{max} = E_\ell\ c/L$, where E_ℓ is the available laser energy determined by the initial population inversion. The radiation decays exponentially with a time constant $t_e = (L/c)/t$, where t represents the fraction of radiation lost to the mirrors per pass. In order to test this behavior, a preliminary scattering experiment was performed. The experimental set-up is shown in Fig. 20. The laser could be run with either an R = 10 meter, 65% reflecting output mirror or an R = 10 meter, 99% reflecting mirror. The cavity length, L, could be set at 1.93 meters or 3.45 meters. To measure the intra-cavity radiation density, a 1 mil tungsten wire was suspended in the beam. The scattered radiation from the wire was detected by a gold doped germanium photoconductive detector. With the 65% mirror in place, a photon drag detector was used to measure the laser output pulse shape as a check on the intra-cavity detector. A measurement was also made in this case of the total energy output with a bolometer, which gives E_ℓ. An aperture was placed in the cavity causing oscillation in the TEM_{20} mode.

The laser was first operated in the open cavity configuration and the mirror adjustments were optimized to obtain maximum power with a good output mode. Figure 21a shows a typical pulse with L = 1.93 m measured with the intra-cavity detector (in good agreement with the photon drag detector). The FWHM is 110 nanoseconds. The low level output at longer times is due to repopulation of the CO_2 by nitrogen molecules. Keeping everything else constant, the output mirror was replaced by a totally reflecting (~ 99%) mirror. An 80% attenuator was placed in front of the detector to prevent saturation. Because of slight differences in the mirrors, the alignment was readjusted by trial and error to achieve maximum power and pulse length. Figure 21b shows typical closed cavity results.

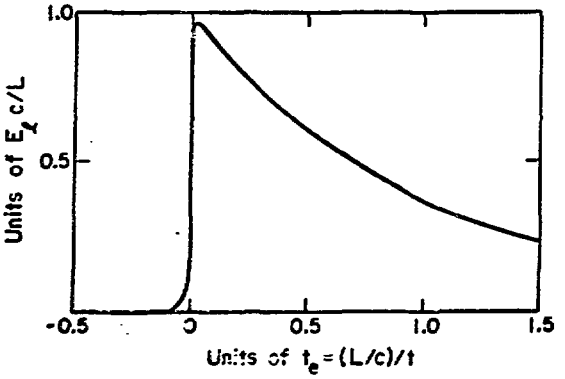

Fig. 19. Intra-cavity power

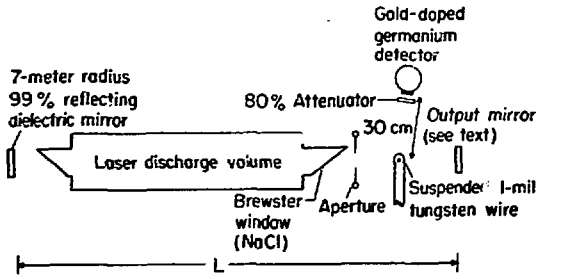

Fig. 20. Closed cavity experimental setup.

The maximum power level has increased by a factor of 3.8. The FWHM is 210 nanoseconds while the long term decay time is t_e = 650 nanoseconds. Another experiment was performed with L = 3.45 m. The closed cavity result is shown in Fig. 21c. The relative power increase was 2.2, the FWHM equaled 500 nanoseconds and the long term decay time was t_e = 720 nanoseconds.

The above results agree with the following analysis, if it is remembered that a part of the energy due to nitrogen repopulation will be somewhat delayed. It will be assumed that, with everything else kept constant, E_ℓ is the same in both cases. In the open cavity result of Fig. 21a, the energy equals about 0.8 joules. An analysis of the pulse measured with the photon drag detector shows that the maximum output power in this case is about 5 megawatts. The intra-cavity power is given approximately by P(inside) = 2P(outside)/(1-R). For R = .65, P(inside) = 29 megawatts. The intra-cavity power in Fig. 21b is estimated to be P(inside) = (0.8 joules)2/(1.93 meters), or 125 megawatts. The predicted increase in intra-cavity

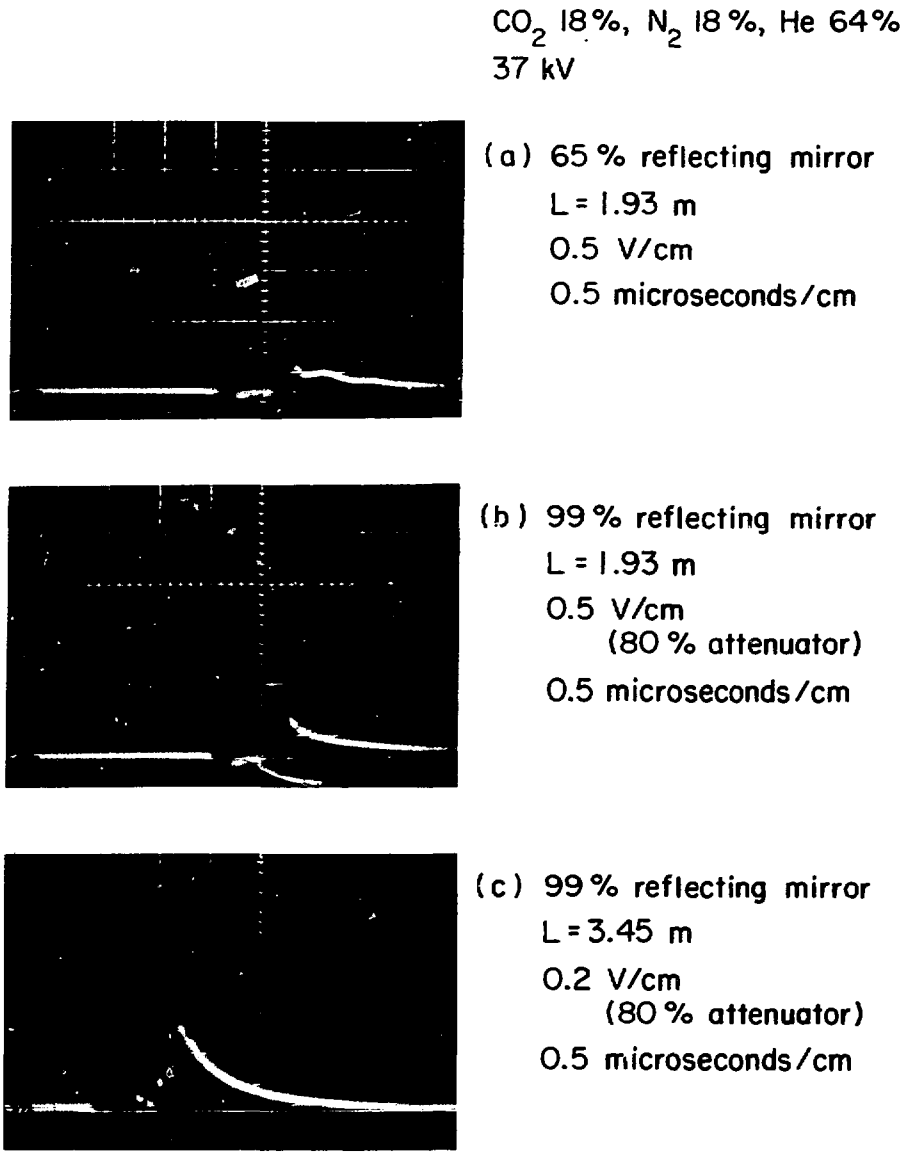

Fig. 21. Closed cavity experiments.

power is 4.3. The useful laser power increases by a factor of 25. For the 3.45 meter cavity, the predicted increase is a factor of 2.4, and from t_e, t = 1.6%, a reasonable figure considering losses from the mirrors, imperfections in the Brewster windows, and the wire. The t_e for the 1.93 m cavity is somewhat longer than expected, probably due to nitrogen repopulation.

During the tuning of the closed cavity, off-axis modes were obtained with very high peak powers (>200 megawatts) but with large diffraction losses indicated by sparking on the aperture. The laser energy was purposely kept low by using a lean gas mixture. Even so, the coating was completely burnt off a gold coated copper mirror (R = 98.5%). Dielectric mirrors held up well at the highest power densities. They are presently reported to withstand 500 megawatts/cm^2 (pulsed). A laser sufficient to give 200 megawatts for a scattering experiment need only have ~ 1 joule available energy and

an active volume of about .06 litres.

D. CO_2 Laser Development

In order to initiate a program of infrared laser diagnostics in the Sherwood program at L.A.S.L., a program of laser development has been carried out. The result is a laser of novel design which remedies some of the difficulties inherent in the promising Pearson-Lamberton[13] configuration. A cross-section of the laser is shown in Fig. 22. The main discharge takes place at atmospheric pressure between a Rogowski profile electrode and a flat mesh (or two Rogowski electrodes). If the main gap is preionized and the discharge takes place fast enough, a glow discharge without arcs can be obtained. The fast pulse (FWHM = 100 nanoseconds) is obtained from a low inductance capacitor bank. Pre-ionization occurs by means of fine tungsten wires located behind the mesh, capacitively coupled to ground. When a rising positive pulse is applied to the mesh, an initial discharge takes place between the mesh and the wires. Ultraviolet produced in the discharge travels through the mesh and causes surface photoemission from the cathode. It has been found that the resulting glow discharge is localized around the area of the cathode illuminuated by the wires. Therefore, it is possible to shape the discharge in one dimension by the placement of the wires.

Parameters of the first laser constructed and one currently under construction are given in Table I. The first laser was used in holographic interferometry experiments and the closed cavity experiments mentioned above. Its closed gas system prevented helium waste and allowed reproducible experiments over a week or more between fillings. The laser currently under construction is shown in Fig. 22. The parameters in Table I are given for one unit. These can be used singly or stacked longitudinally. Three units can be stacked at 120° with respect to one another to form a laser which favors cylindrically symmetric modes. The units can be run with small spacings and only the center wires activated to produce lower order modes for closed cavity scattering experiments. For applications such as interferometry calling for more energy, the spacing can be increased and the external wires activated to achieve the maximum excited volume.

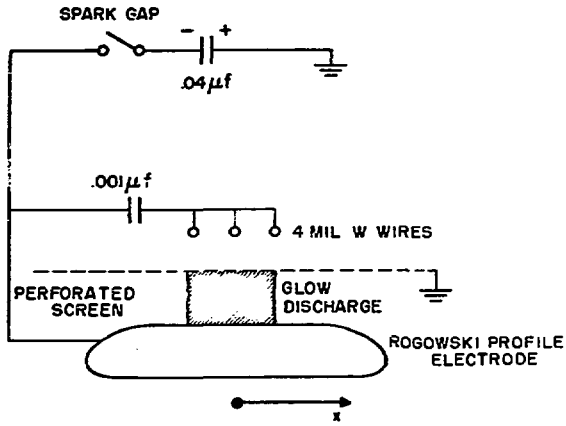

Fig. 22. Cross-section of double discharge laser.

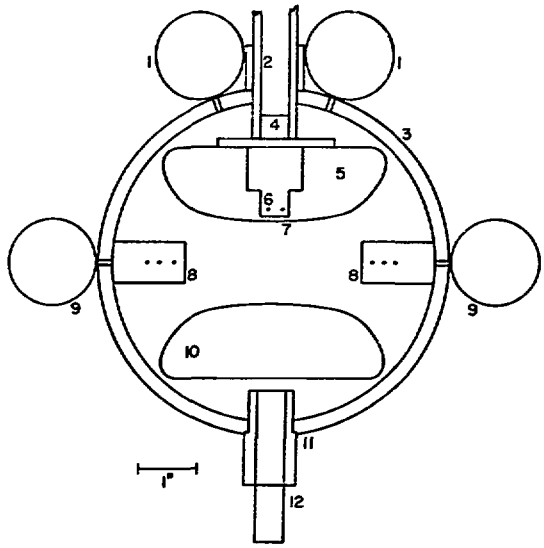

Fig. 23. CO_2 Laser II, Cross-section.

1. Primary discharge capacitors - center wires.
2. Lucite coaxial cable recepticle.
3. Six inch O.D. lucite tube.
4. Spacer to adjust main gap.
5. Hollow Rogowski profile electrode, anode.
6. Primary discharge wires - 4 mil tungsten.
7. Brass mesh with 45% open area.
8. Outer primary discharge wire holders.
9. Primary discharge capacitors - outer wires.
10. Solid Rogowski profile electrode, cathode.
11. Compression gland.
12. Movable rod for adjusting main gap.

TABLE I. LASER PARAMETERS

	LASER 1	LASER 2 (Under construction)
ELECTRODE CONFIGURATIONS	100 cm x 10 cm Rogowski surface vs. flat mesh. 2.5 cm spacing	Two 71 cm x 7 cm Rogowski surfaces with incorporated mesh. 3.8 cm spacing.
WIRES	2 wires 1 cm from centerline	2 wires 0.5 cm from centerline. 2 optional Pearson-Lamberton wires.
MAIN CAPACITOR	.06 microfrads, 45 kV	.075 microfarads. 70 kV Marx generator
COUPLING CAPACITOR	.0015 microfarads	.001 microfarads
GAS SYSTEM	Closed, convective	Closed, recirculating
OPTIMUM GAS MIXTURE	CO_2: .30, N_2: .30, He: .40	-
PULSE LENGTH	100 nanoseconds	-
MAXIMUM OUTPUT ENERGY	4 joules	8 joules (expected)
VOLUME EFFICIENCY	17 joules/litre	-
ENERGY UTILIZATION EFFICIENCY	6.3%	-
PULSE ENERGY REPRODUCIBILITY	$\pm$ 3%	-

ACKNOWLEDGEMENTS

I would like to thank B. R. Suydam for his suggestions on the calculation of self-consistent laser modes. I would also like to thank P. R. Forman for his advice on the laser construction and scattering experiments.

REFERENCES

1. J. W. Dawson, et. al., "Controlled Fusion Using Long Wavelength Laser Heating with Magnetic Confinement", Paper No. CN-28/D-13, IAEA Conference, Madison, Wisconsin June 1971.

2. S. Humphries, Jr., "Multiple-Pass Laser Heating of a Magnetically Confined Plasma", LA-5010, Los Alamos, New Mexico, October 1972.

3. J. Tulip, et. al., "Intercavity Radiation-Induced Air Breakdown in a TEA CO_2 Laser", Appl. Phys. Lett. 19, No. 10, 433, (1971).

4. D. L. Jassby and M. E. Harhic, "Thermal Decay of an Infrared-Laser Heated Arc Plasma", UCLA-34-P-157-X-4, University of California, Los Angeles, March 1972.

5. J. E. Geusic, et. al., "Continuous 0.53-μm Solid-State Source Using $Ba_2NaNb_5O_{15}$", IEEE J. Quantum Electron., QE-4, 353 (1968).

6. H. Kogelnik and T. Li, "Laser Beams and Resonators", Appl. Opt. 5, No. 10, 1550 (1966).

7. A. E. Seigman, "Unstable Optical Resonators for Laser Applications", Proc. IEEE, 53, 277 (1965).

8. A. G. Fox and T. Li, "Modes in a Maser Interferometer with Curved Mirrors", Quantum Electron. III, New York: Columbia University Press, 1964, 1263.

9. S. I. Braginskii, "Transport Processes in a Plasma", Reviews of Plasma Physics, Vol. 1, New York: Consultant's Bureau, 1965, 205.

10. A. Yariv, Introduction to Optical Electronics, New York: Holt, Rinehart and Winston, Inc. 1971, 37.

11. G. C. Vlases, "Heating of Pinch Devices with Lasers", Phys. Fluids, 14, 1109 (1971).

12. A. W. DeSilva and G. C. Goldenbaum, "Plasma Diagnostics by Light Scattering", Methods of Experimental Physics, Vol. 9, Part A, New York, Academic Press, 1970, 61.

13. P. R. Pearson and H. M. Lamberton, "Atmospheric Pressure CO_2 Lasers Giving High Output Energy Per Unit Volume", IEEE J. Quantum Electron., QE-8, 145 (1972).